Light-Scattering Photometer with Optical Microscope for the In-Line Study of Polymer Extrusion

S. LI, K. B. MIGLER, E. K. HOBBIE, H. KRAMER, C. C. HAN, E. J. AMIS

Polymers Division, National Institute of Standards and Technology, Building 224, Room B210, Gaithersburg, Maryland 20899

ABSTRACT: A light-scattering photometer with optical microscope for in-line studies during polymer processing is described. The instrument utilizes a commercial twin-screw extruding device that feeds molten polymer into a narrow slit die equipped with sapphire optical windows. The flow rate through the die is controlled via the feed rate, screw rate, and a by-pass valve. The optics for light scattering and microscopy can be switched back and forth via simple translation of a rail-mounted optical platform without realignment, allowing efficient *in situ* morphological studies in both real and reciprocal space. Extruded polystyrene/polyethylene blends and melts are used to demonstrate the performance and versatility of the instrument. © 1997 John Wiley & Sons, Inc. J Polym Sci B: Polym Phys **35**: 2935–2943, 1997
Keywords: polymer blend, extrusion, light scattering, optical microscopy

INTRODUCTION

Most homopolymer melts are immiscible, and polymer processing techniques often rely on mechanical mixing devices to "blend" thermodynamically incompatible components. Extrusion is a particularly common and effective way of producing fine dispersions out of immiscible polymers. Such blends form multiphase domain structures for which the specific domain morphology plays an important role in the physical characteristics of the resulting material, and knowledge of the structures induced during processing is thus quite useful.[1–15] Although the technique of rapidly quenching the extrudate and studying the frozen-in morphological characteristics has been a widely used and powerful approach, in some applications it is desirable to have more direct access to the blend during processing.

Two common experimental methods used for studying the phase behavior of polymer blends are light scattering and optical microscopy. When combined together, these techniques can provide structural information over a wide range of length scales in both reciprocal and real space. Our group recently reported the development of a light-scattering photometer with an optical microscope for studying polymer blends under simple shear flow.[16] In this article we describe an instrument of similar capabilities designed for *in situ* studies of polymer extrusion. We demonstrate the use and versatility of the instrument on low-volume fraction dispersions of polystyrene and polyethylene. Also, we measure the flow field within the slit die as a function of bulk flow rate via optical tracking of silica microspheres dispersed in pure polystyrene and polyethylene melts.

INSTRUMENT

The extrusion is carried out using a Haake Rheocord 9000* with a corotating conical twin-screw attachment. Figure 1 shows a side view of the extruder and slit die. By necessity, the instrument must accommodate the high pressures encountered during polymer processing. Figure 2 shows
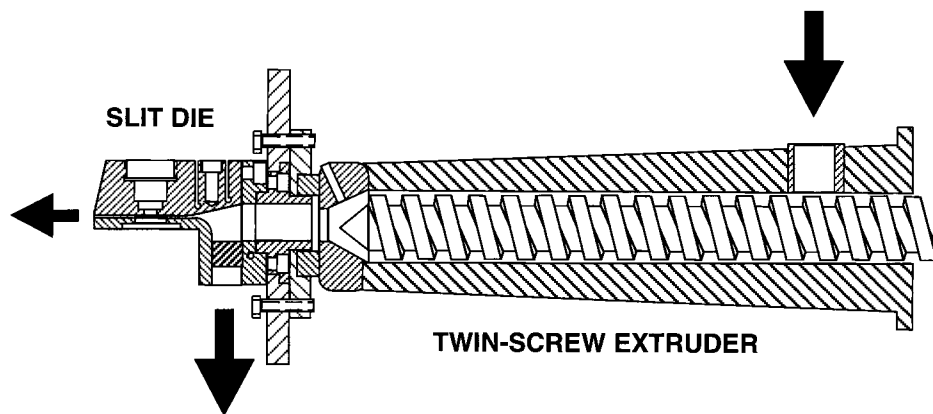
Figure 1. Side view of the conical twin-screw extruder and slit die. Polymer fed into the barrel flows out through the slit die and by-pass valve. Sapphire optical windows in the slit die allow in-line studies during processing.

a cut-away view of the stainless steel slit die equipped with upper and lower sapphire optical windows that can easily accommodate pressures over 20 MPa without cracking. The width of the slit can be adjusted from 0.2 to 1.0 mm, and the diameter of the optical windows is 12 mm. Temperature can be controlled to within ±1 Kelvin at the die and at three zones along the extruder barrel. The Haake device also controls the screw rate and monitors the channel pressure and torque supplied by the motor. The feed rate into the barrel is metered externally. There are shear stresses arising from both channel flow within the die and mixing flows that take place in the barrel. A by-pass valve allows us to externally control the amount of material flowing through the die so as to isolate either of these two effects.

Figure 3 shows a schematic of the light-scattering photometer component, and Figure 4 shows a schematic of the optical microscope component. The latter provides real-space images of objects down to sizes on the order of 1 μm, and the former can extend this down to sizes on the order of 100 nm in reciprocal space. Each component is interfaced to a PC via two separate CCD cameras. Switching back and forth between real space and reciprocal space is accomplished by the translation of a rail-mounted optical frame, to which is fastened the optical objective, polarizing filter, two mirrors, and screen. The rail is mounted on an aluminum frame that is attached to the table and which supports the slit die, which is in turn attached to the barrel of the extruder.

Light Scattering

The light source for the scattering experiments is a vertically polarized 5 mW He-Ne laser (λ = 632.8 nm). The beam enters from the side and is reflected down through the die, where the scattered light illuminates a flat translucent screen. The maximum angular range of the optics allowed by the slit die is ±45°, with a ±30° working range of useful scattering angles. An image of the screen is formed on a CCD detector by a macro lens and a second mirror. Holes in the center of the screen and second mirror allow passage of the primary beam. With the camera aperture manually set at the desired diameter, the shutter speed, the number of accumulations, the pixel-array dimensions, and the data format are all adjusted to achieve the best possible image quality via a computer interface using commercially available software. The transmitted beam intensity is monitored externally. Light-scattering images are collected at 512 × 512 pixel resolution, averaged together to achieve good statistics, and then reduced to 256 × 256 for analysis.

Microscope

The illumination source for microscopy is a Xenon flash lamp (EG & G, FYD-1130) which minimizes smearing due to either high flow rates or vibrations. The length of the flash pulse is approximately 0.3 μs, and the timing of the pulses is controlled with an external circuit connected to a flash-lamp power supply (EG and G electrooptics PS-1110). The flash rate is normally set to be in synch with the video frame acquisition rate of 30 frames per second.[17] A faster rate leads to multiple images on a given frame, which can be utilized for determining particle speeds at high flow rates.

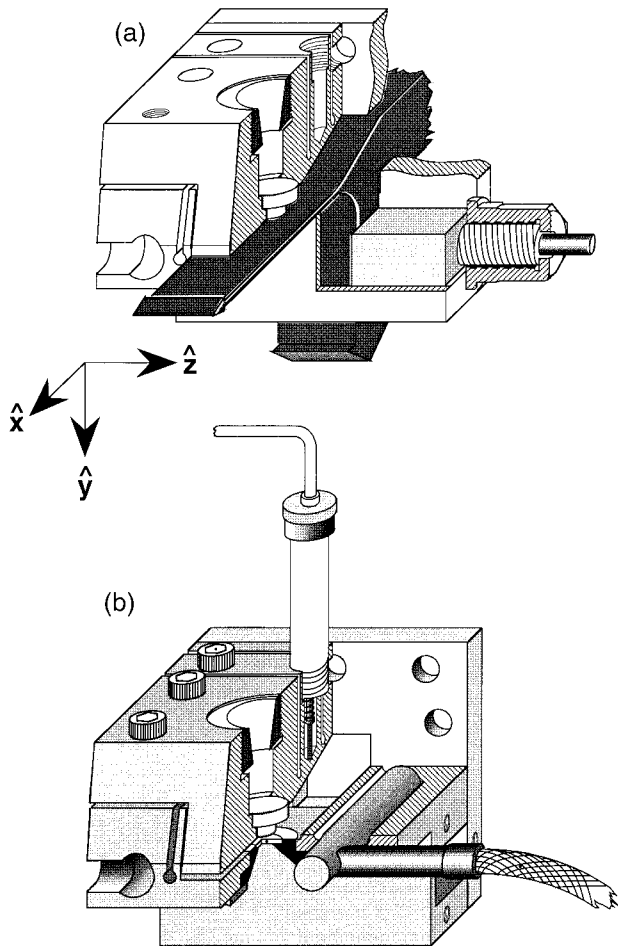To facilitate the observation of objects with

Figure 2. (a) Cut-away schematic of the die showing the flow of the sample through the channel and by-pass valve. (b) Cut-away schematic of the die that shows the sapphire windows, heating element, and thermocouple sensor for temperature control. The flow through the slit die is in the x direction, with the velocity gradient in the y direction and vorticity in the z direction. Sapphire optical windows in the top and bottom of the die permit optical monitoring during processing. The light-scattering measures the projection of the structure factor onto the x-z plane. The focal plane of the microscope is parallel to this plane and can be adjusted as a function of y.

similar indices of refraction, the instrument utilizes a phase-contrast microscope of the Zernike type.[18–21] Because the image represents spatial variations in refractive index, the square-amplitude of the Fourier spectrum can be compared directly with the pattern of scattered light. The phase ring can also be removed for conventional bright-field microscopy. A long working distance, $25\times$ objective with a numerical aperture of 0.35 is mounted below the die. A polarizing filter between the objective and the eyepiece corrects for birefrin-

gence arising from the sapphire windows. The image is then passed through a relay lens to a CCD video camera (Dage MTI, model 72) which is interfaced to a PC and a super-VHS video recorder. A frame grabber (DT-3851) is used to digitize an image of 640×480 pixels and save it in binary format. The eyepiece and relay lens are not essential optical components, as the image from the objective can be formed directly onto the CCD array.

CALIBRATION

Scattering Angle and Intensity

To calibrate the scattering angle, we used computer-generated families of concentric rings of known radial increment. With the optics properly aligned, the ring grating is centered on the beam within the plane of the screen. Because the CCD captures the focused image of the screen, the mapping of the grating dimensions onto the pixel array and the measured distance between the scattering cell and the screen give the scattering angle in air in terms of pixel number x_i [Fig. 5(a)], which over the range of interest is well represented by $\theta'(x_i) \approx 0.0015 + 0.0068(x_i) - 1.112 \times 10^{-5}(x_i^2)$ within a 2% uncer-
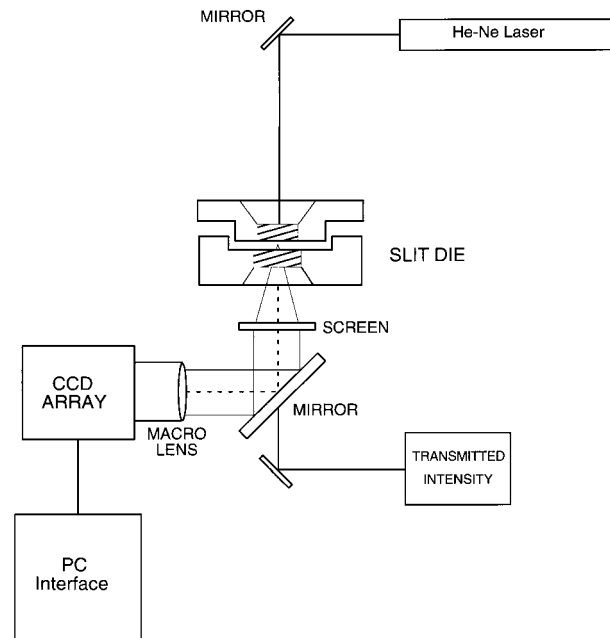

Figure 3. Schematic diagram of the light-scattering component. The image of the scattered light that appears on the screen is recorded with a CCD camera that is interfaced to a PC.
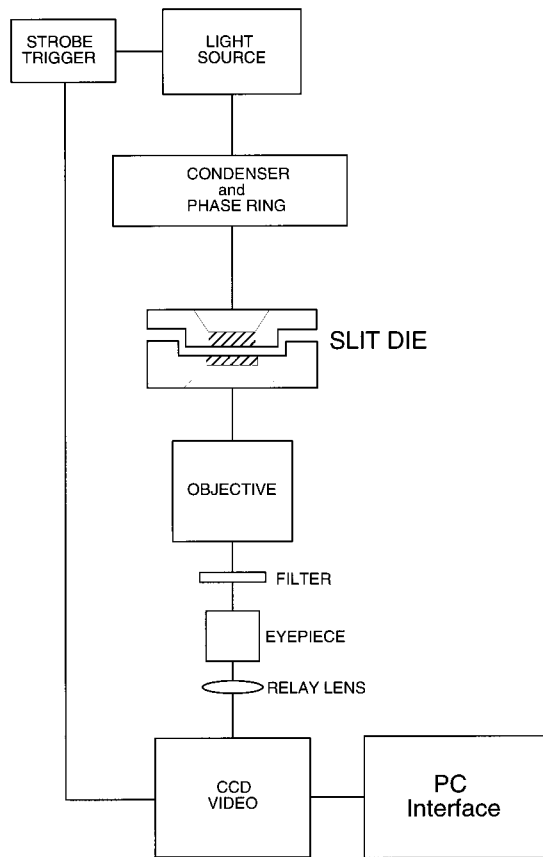
Figure 4. Schematic diagram of the microscope component. Because the sapphire windows are birefringent, a polarizing filter is needed between the objective and the eyepiece to restore optical clarity. The phase ring may be removed depending on the application.

tainty. The relation between scattered wavevector and x_i is then

$$q = \frac{4\pi}{\lambda} \sin\left\{ \frac{1}{2} \sin^{-1}\left(\frac{\sin \theta'(x_i)}{n_p} \right) \right\} \qquad (1)$$

where n_p is the index of refraction of the sample and λ is the wavelength of light within the sample. The calibration curve for $n_p = 1.5$ is shown in Figure 5(b) and is well described by $q(x_i) = A + Bx_i + Cx_i^2$, where $A = 0.001138$ μm^{-1}, $B = 0.06825$ μm^{-1}, and $C = -13.985 \times 10^{-5}$ μm^{-1} within a 2% uncertainty.

To measure the flat-field correction, we placed a quartz sample cell above the screen in the horizontal plane defined by the slit die. Nile Blue A dye at 100 mg/l dissolved in a 50/50 by volume EtOH/H$_2$O solution was placed in the cell and the sample illuminated with the 5 mW He-Ne laser.

A cutoff filter (Schott Glass Technologies Inc. RG-655) was placed between the camera and the screen so that only the fluorescence intensity was measured by the CCD detector. The intensity variation with pixel then gives an isotropic correction factor as a function of x_i that is well represented by $f(x_i) \approx 0.328 + 0.01277(x_i) - 8.268 \times 10^{-5}(x_i^2) + 1.897 \times 10^{-7}(x_i^3)$ within a 6% error.

Microscope

The magnification was measured using a dilute suspension of silica microspheres in a polystyrene melt. The microspheres were obtained from Duke Scientific (NIST Traceable Silica Particle Size Standard, D = 1.58 ± 0.06 μm, $\sigma = \pm 0.04$ μm) and were dispersed in a matrix of polystyrene (DOW Chemical PS 612, $M_w = 192 \times 10^3 M_n = 83 \times 10^3$)
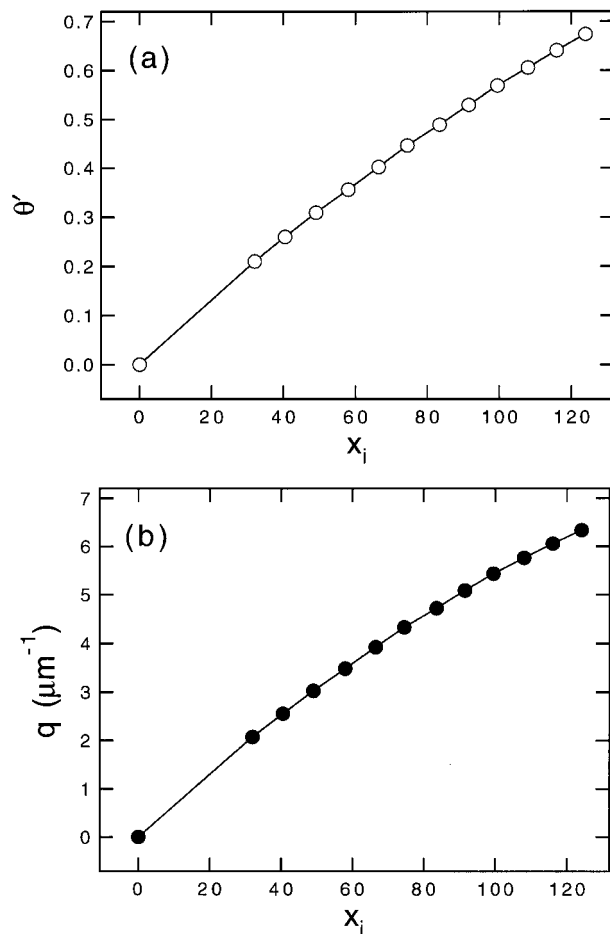

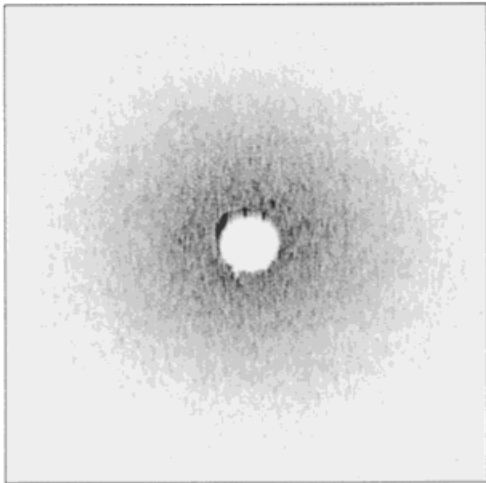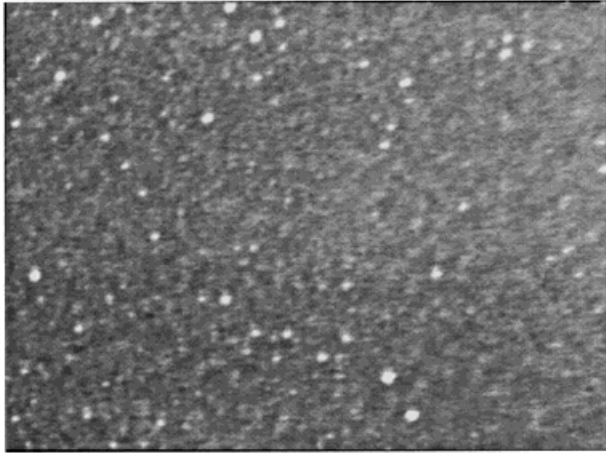**Figure 5.** (a) Measured scattering angle (θ' in radians) vs. pixel number x_i, (b) scattered wavevector q vs. x_i for $n_p = 1.5$.

APPLICATIONS

Blend Morphology

To demonstrate the capabilities of the instrument, we consider extruded dispersions of polyethylene (DOW Chemical LDPE 993I, $M_w = 85.2 \times 10^3$ $M_n = 15.4 \times 10^3$) and polystyrene (DOW Chemical PS 612, $M_w = 192 \times 10^3 M_n = 83 \times 10^3$). Figure 6 shows a light-scattering micrograph pair for an extrusion of 500 : 1 PS : PE by weight prepared at a screw rate of 10 RPM at 175°C with the by-pass valve closed. The extruder has been turned off and the material is at rest in the slit die. The extrudate was slightly turbid, with a transmission factor of 0.5 relative to pure PS.
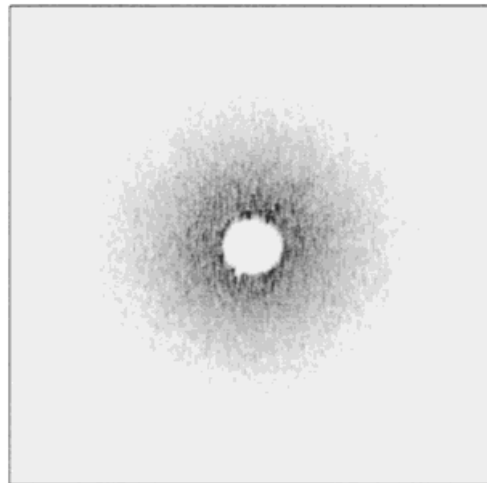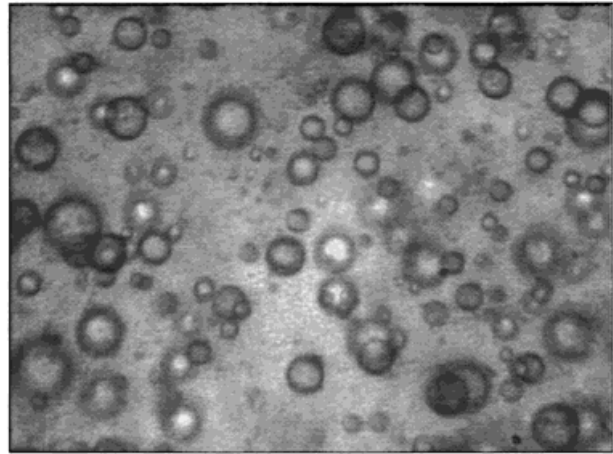

Figure 6. Light-scattering/digital-video-micrograph pair for a dilute extrusion of polyethylene dispersed in polystyrene at $T = 175$°C as described in the text. The width of the micrograph from left to right is 200 μm, and the width of the light-scattering image corresponds to a scattering angle of roughly ±40 degrees. The blend is at rest in the slit die, with the x direction from right to left, the z direction from top to bottom, and the y direction into the page.

at 175°C. A micrometer screw adjustment with coarse and fine settings moves the objective up and down to focus on a given plane within the sample. Calibration of the out-of-image plane dimension was made by directly measuring the width of the slit die, finding the micrometer settings where the top and bottom surfaces of the lower and upper sapphire windows came into focus, and assuming a linear relation between setting and distance over the width of the die. The width of the slit die was set at 0.43 mm for all of the measurements described in this article.

Figure 7. Light-scattering/digital-video-micrograph pair for a dilute extrusion of polystyrene dispersed in polyethylene at $T = 175$°C. The geometry is as specified in Figure 6.

Transients associated with shear stresses caused by flow within the slit die and barrel have died out, leaving an isotropic, polydisperse distribution of PE spheres in a matrix of PS. The micrograph is a phase-contrast image. The light-scattering image shown is a single frame collected at a shutter speed of 0.025 s.

Figure 7 shows a light-scattering micrograph pair for an extrusion of 1 : 100 PS : PE by weight again prepared at a screw rate of 10 RPM at 175°C with the by-pass valve closed. The extruder has been turned off and the material is again at rest in the die. The hot extrudate was moderately turbid, with a transmission factor of 0.3 relative to pure PE. Shortly after cessation of flow, the mixture is a polydisperse, isotropic distribution of PS spheres in a matrix of PE. Because of the droplet size, the PS spheres are clearly evident in the bright-field micrograph (phase ring removed) shown in Figure 7. The difference in domain size between the PS-rich and PS-poor cases is primarily a result of the higher PS viscosity, which leads to higher shear stresses in the PS matrix at a comparable flow or mixing rate.[22]

Figure 8 shows circular averages of the light-scattering data from Figures 6 and 7. The lines are fits to the Debye expression for the angular scattering due to randomly distributed droplets of random size.[23]
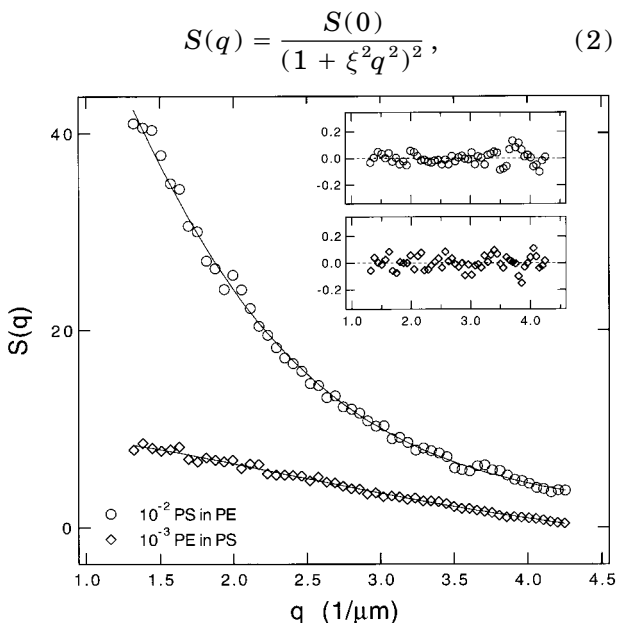
$$S(q) = \frac{S(0)}{(1 + \xi^2 q^2)^2}, \qquad (2)$$

Figure 8. Structure factor as a function of wavevector from a circular average of the data from Figures 6 and 7. The lines are fits to eq. (2), with deviation plots between fit and data shown in the insets.

with the insets showing the fractional deviation between data and fit. Note that eq. (2) gives $S(q) \sim q^{-4}$ at high q, consistent with sharp interfaces. The quantity ξ should scale as the volume fraction of the "dispersed" phase divided by the surface area per unit volume.[23] From the fit we get $\xi_a = 0.19$ μm for the data in Figure 6 and $\xi_b = 0.48$ μm for the data in Figure 7. The length scale ξ should scale as $\langle R^3 \rangle / \langle R^2 \rangle$, where the brackets denote an average over the size distribution. From the optical micrographs, the large end of the distribution in Figure 6 corresponds to a diameter of around 5 μm, while that in Figure 7 corresponds to 18 μm. In reciprocal space, these dimensions are behind the beam stop. In both cases, a significant fraction of droplets are too small to be visible in the micrographs. This was confirmed using SEM on quenched extrudate of the PE rich blends, which revealed the submicron structure. Although multiple scattering effects will make ξ artificially small in high-contrast systems,[24] we find reasonable agreement between the values of ξ obtained from the fitting and the droplet dimensions at the small end of the size distribution.

Flow and Viscous-Stress Fields

As another demonstration of the instrument, we use optical tracking of silica microspheres (Duke Scientific, NIST Traceable Silica Particle Size Standard, $D = 1.58 \pm 0.06$ μm, $\sigma = \pm 0.04$ μm) in pure PS and PE melts to map the flow field within the slit die. Silica microspheres were dispersed in PS and PE melts at volume fractions of 10^{-4}. At this low composition the presence of the "filler" will not appreciably alter the flow field of the melt. We tracked the positions of the sphere centers as a function of time and position within the die for different bulk flow rates. The flow rates were determined by weighing the amount of extrudate that passed through the die in a measured interval of time. The flow field for a pure PS melt at $T = 175$°C is shown in Figure 9. The inset shows the field close to the bottom window. The flattening of the velocity profile with increasing flow rate is due to shear thinning and the transition to plug-like flow. The lines in the main figure are fits with the expression characterizing channel flow[25]

$$v(y) = v_o \left[1 - \left\{ \frac{|y - d/2|}{d/2} \right\}^\alpha \right] \qquad (3)$$

where y is the vertical position within the die, d is the die width, and v_o is the velocity at the center
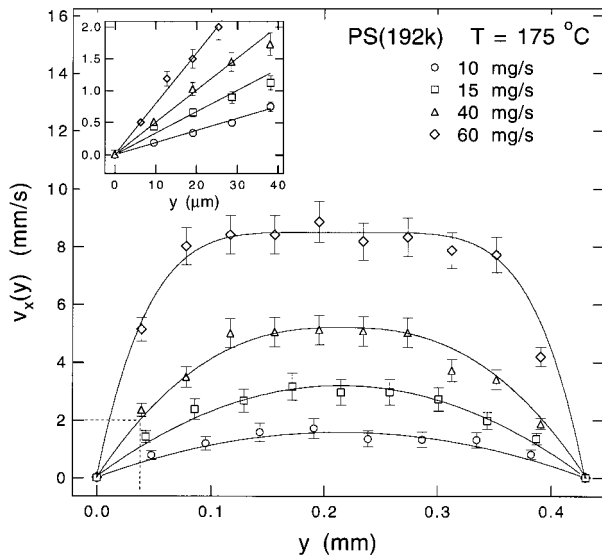
Figure 9. Velocity profile as a function of position within the slit die for a pure polystyrene melt as measured with the optical-tracking technique described in the text. The curves are fits to eq. (3), and the inset shows an expanded plot of the flow profile next to the bottom wall. The measured flow rates are given in milligrams per second.

of the die. The exponent α is related to the power-law index n via $\alpha = 1 + 1/n$. The lowest two profiles (10 mg/s and 15 mg/s) are parabolic ($\alpha = 2$, $n = 1$), the second highest (40 mg/s) corresponds to $\alpha = 2.5$ ($n = 0.67$), and the highest (60 mg/s) corresponds to $\alpha = 4.7$ ($n = 0.28$). The lines
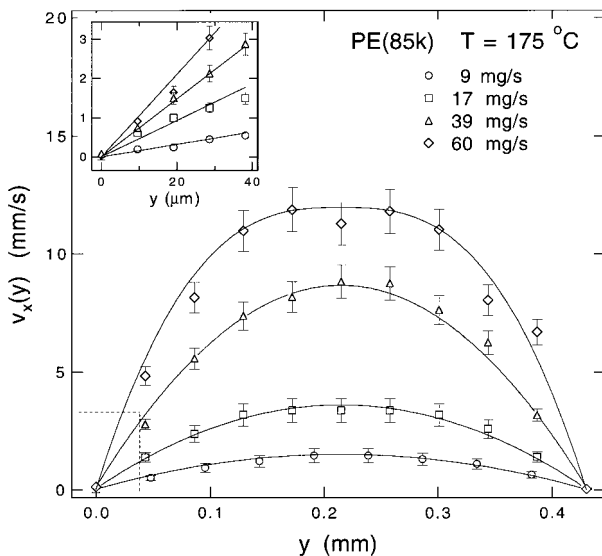

Figure 10. A plot similar to Figure 9 for a pure polyethylene melt.

in the inset are linear (simple-shear) approximations to the local profile by the wall.

Figure 10 shows a similar plot for a pure PE melt at $T = 175°C$. The PE is more Newtonian over a comparable range of flow rates, with parabolic profiles ($\alpha = 2$, $n = 1$) for 9 mg/s, 17 mg/s, and 39 mg/s, and $\alpha = 2.8$ ($n = 0.56$) for 60 mg/s. The inset again shows the flow condition near the bottom window, with the lines representing linear fits to the local velocity profile. The rate-of-strain and vorticity tensors are, respectively, symmetric and antisymmetric combinations of the dyad $\vec{\nabla}v = (\partial v_x/\partial y)\hat{y}\hat{x}$, where $\hat{x}$ defines the direction of flow and $\hat{y}$ defines the gradient direction. Figure 11 shows the velocity gradient $\partial v_x/$
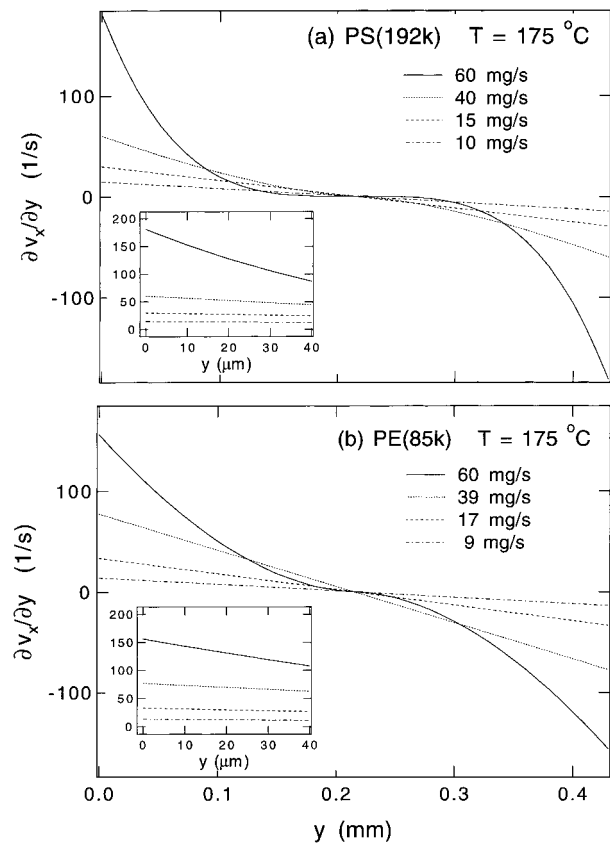

Figure 11. Velocity gradient as a function of position within the slit die for (a) a pure polystyrene melt and (b) a pure polyethylene melt at $T = 175°C$ as determined from the fits of the velocity profiles to Eq. (3). The insets show the behavior in the vicinity of the bottom wall. If one approximates the local flow condition as simple shear, then these plots give the effective shear rate as a function of position within the slit die. Note that shear thinning leads to regions of high shear stress by the walls and regions of zero shear stress in the middle ("plug flow") at high flow rates.
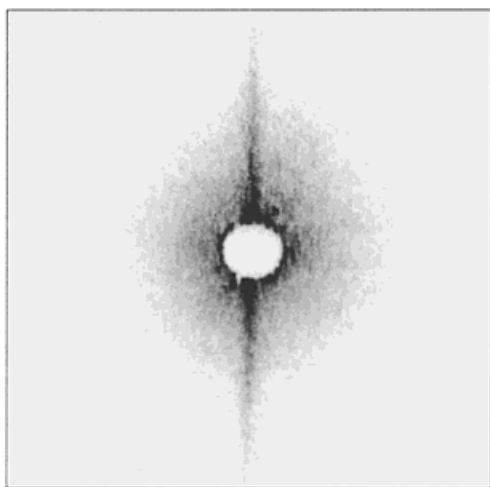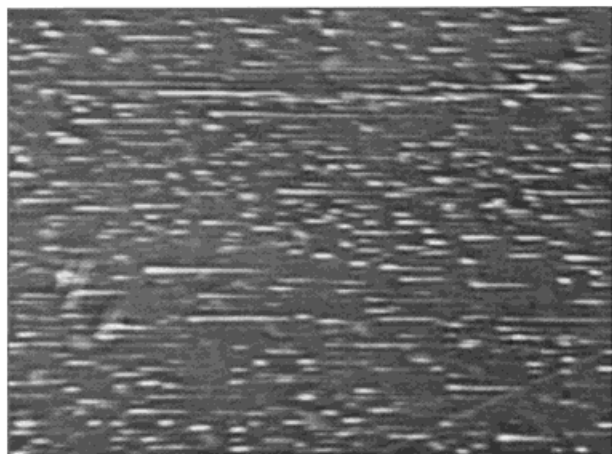
Figure 12. Light-scattering/micrograph pair for a dispersion of 2×10^{-3} weight fraction PE in PS at $T = 175°C$ and a local shear rate of 60 s^{-1}. The geometry is as specified in Figure 6, with the flow direction from right to left and the velocity-gradient (y) direction into the page. The morphology corresponds to a narrow (less than 50 μm thick) layer of blend in the high-shear region by the walls with pure PS melt filling the rest of the slit die.

∂y as a function of position within the slit die as determined by differentiating the fits to the velocity profiles shown in Figures 9 and 10. The insets show the behavior close to the windows. If we make the local approximation of simple shear, then these plots give the effective shear rate $\dot{\gamma}(y)$ within the die.

Approximating Simple Shear Flow

Because of the variation of the effective shear rate within the slit die, the domain structure depends on position. This somewhat complicates the mor-

phology of two-phase channel flow. In an attempt to get around this, we can exploit the nature of the flow profile to locally mimic conditions that resemble simple shear. By adding pure melt corresponding to the matrix during the blend extrusion process, the channel-flow profile, with a high flow rate in the middle and limited flow by the walls, leads to isolated regions of blend next to the walls with pure melt filling the rest of the channel. By optically monitoring the thickness of this blended layer with the microscope, we can isolate a thin high-shear-stress region next to the window. As shown in Figures 9 and 10, the flow profile in the immediate vicinity of the wall can be approximated to leading order by simple shear.

Figure 12 shows a light-scattering/micrograph pair for dispersion of PE in PS (2×10^{-3} weight fraction) at $T = 175°C$. From a measurement of the bulk flow rate, and based on the data shown in Figures 9 and 11, we estimate the local shear rate to be approximately 60 s^{-1}. In this case, the highly elongated domains arise from the relatively high viscosity of the PS matrix with respect to the PE droplets.[22] The highly anisotropic domain structure is inverted in q space and is evident as dark vertical streaks in the light-scattering pattern. Although this technique is somewhat crude, it offers a convenient and relatively quick way to study the high-shear morphology of non-Newtonian materials at high temperatures and flow rates. It is also an efficient way to get light-scattering/microscopy image pairs from highly turbid materials.

CONCLUSIONS

In conclusion, we describe a light-scattering/microscopy instrument for in-line studies of polymer extrusion. We demonstrate the performance of the instrument on low-volume fraction dispersions of extruded polystyrene and polyethylene, and by mapping the flow field as a function of bulk flow rate within the slit die for pure polystyrene and polyethylene melts. The instrument should prove to be a useful probe of polymer-blend morphology and hydrodynamics during processing.

dation or endorsement by the National Institute of Standards and Technology, nor does it imply that materials or equipment identified are necessarily the best available for the purpose.

REFERENCES AND NOTES

1. S. L. Sakellarides and A. J. McHugh, *Polym. Eng. Sci.,* **27,** 1662 (1987).
2. T. I. Ablazova, M. B. Tsebrenko, A. B. V. Yudin, and G. V. Vinogradov, *J. Appl. Polym. Sci.,* **19,** 1781 (1975).
3. M. V. Tsebrenko, A. V. Yudin, T. I. Ablozova, and G. V. Vinogradov, *Polymer,* **17,** 831 (1976).
4. N. R. Krasnikova, E. V. Kotova, G. V. Vinogradov, and Z. Pelzbauer, *J. Appl. Polym. Sci.,* **22,** 2081 (1978).
5. G. V. Vinogradov, N. R. Krasnikova, V. E. Dreval, E. V. Kotova, and E. P. Plotnikova, *Int. J. Polym. Mater.,* **93,** 187 (1982).
6. V. E. Dreval, G. V. Vinogradov, E. P. Plotnikova, M. P. Zabugina, N. P. Krasnikova, E. V. Kotova, and Z. Pelzbauer, *Rheol. Acta,* **22,** 102 (1983).
7. M. P. Zabugina, E. P. Plotnikova, G. V. Vinogradov, and V. E. Dreval, *Int. J. Polym., Mater.,* **10,** 1 (1983).
8. C. D. Han and T. C. Yu, *J. Appl. Polym. Sci.,* **15,** 1163 (1971).
9. C. D. Han and T. C. Yu, *Polym. Eng. Sci.,* **12,** 81 (1972).
10. K. Min, J. L. White, and J. F. Fellers, *J. Appl. Polym. Sci.,* **29,** 2117 (1984).
11. B. Liang, J. L. White, J. E. Spruiell, and B. C. Goswami, *J. Appl. Polym. Sci.,* **28,** 2011 (1983).
12. K. Min, J. L. White, and J. F. Fellers, *Polym. Eng. Sci.,* **24,** 1327 (1984).
13. Y. Shimomura, J. E. Spruiell, and J. L. White, *Polym. Eng. Rev.,* **2,** 417 (1983); S. Endo, K. Min, J. L. White, and T. Kyu, *Polym. Eng. Sci.,* **26,** 45 (1986).
14. A. P. Plochocki, *Polym. Eng. Sci.,* **23,** 618 (1983).
15. D. Yu, M. Esseghir, and C. Gogos, *ANTEC '95,* 136 (1995).
16. S. Kim, J. Yu, and C. C. Han, *Rev. Sci. Instrum.,* **67,** 3940 (1996).
17. S. Inoue, *Video Microscopy,* Plenum, New York, 1986.
18. R. F. Smith, *Microscopy and Photomicroscopy / A working Manual,* Chemical Rubber, Boca Raton, FL, 1993.
19. M. Francon, *Progress in Microscopy,* Row, Peterson and Company, Evanston, IL, 1961.
20. T. G. Rochow, *An Introduction to Microscopy by Means of Light, Electrons, X-rays, or Ultrasound,* Plenum, New York, 1978.
21. E. M. Slayter and H. S. Slayter, *Light and Electron Microscopy,* Cambridge University Press, New York, 1993.
22. G. I. Taylor, *Proc. R. Soc. Lond.,* **A146,** 41 (1932); *ibid,* **A146,** 501 (1934).
23. P. Debye, H. R. Anderson, and H. Brumberger, *J. Appl. Phys.,* **28,** 679 (1957).
24. E. K. Hobbie and Lipiin Sung, *Am. J. Phys.,* **64,** 1298 (1996).
25. J. Agassant, P. Avenas, J. Sergent, and P. Carreau, *Polymer Processing: Principles and Modeling,* Hanser, Munich, 1991.

Error bars in graphs represent the best estimate of two standard deviations in experimental uncertainty.